Please cite this article in press as: Li and Minkara, Decoding SP-D and glycan binding mechanisms using a novel computational workflow, Biophysical Journal (2025), https://doi.org/10.1016/j.bpj.2025.04.007

Biophysical Journal
Article

Biophysical Society

Decoding SP-D and glycan binding mechanisms using a novel computational workflow

Deng Li[1] and Mona S. Minkara[1,*]
[1]Department of Bioengineering, Northeastern University, Boston, Massachusetts

ABSTRACT Surfactant protein D (SP-D) plays an important role in the innate immune system by recognizing and binding to glycans on the surface of pathogens, facilitating their clearance. Despite its importance, the detailed binding mechanisms between SP-D and various pathogenic surface glycans remain elusive due to the limited experimentally solved protein-glycan crystal structures. To address this, we developed and validated a computational workflow that integrates induced fit docking, molecular mechanics/generalized Born surface area binding free energy calculations, and binding pose metadynamics simulations to accurately predict stable SP-D-glycan complex structure and binding mechanisms. By utilizing this workflow, we identified primary and secondary binding sites in SP-D critical for glycan recognition and uncovered a calcium chelation mode correlating with high binding affinity. To demonstrate the workflow's utility, we investigated the binding of pilin glycan from *Pseudomonas aeruginosa* (*P. aeruginosa*) to SP-A, SP-D, and mannose-binding lectin (MBL). We found that SP-D exhibited the most stable binding with pilin glycan versus SP-A and MBL, highlighting its potential role in the innate immune response against *P. aeruginosa* infection. These findings deepen our understanding of SP-D's role in the innate immune response and provide a basis for engineering SP-D variants for therapeutic applications. Moreover, our computational workflow can serve as a powerful tool for exploring protein-ligand interactions in diverse, biologically significant systems. It provides a robust framework to guide experimental studies and accelerates the development of novel therapeutics, effectively bridging the gap between computational insights and practical applications.

SIGNIFICANCE Surfactant protein D (SP-D) is a key component of the innate immune system, crucial for recognizing glycans on pathogen surfaces and facilitating their clearance. Despite its importance, the structural details of SP-D-glycan interactions remain unclear due to limited experimental data. This study introduces a novel computational workflow that overcomes these challenges, integrating advanced modeling techniques to predict stable SP-D-glycan complex structures and uncover binding mechanisms. By demonstrating SP-D's more stable binding to pilin glycan from *Pseudomonas aeruginosa*, we highlight its critical role in innate immune function. Our workflow not only enhances understanding of protein-glycan interactions but also provides a versatile tool for exploring biologically significant systems, offering insights to guide experimental research and therapeutic development.

INTRODUCTION

The innate immune system constitutes the body's primary defense mechanism against pathogenic invasion, providing a rapid and nonspecific response to infections (1–3). Central to this system are pattern recognition receptors (PRRs), which identify pathogen-associated molecular patterns on microbial surfaces (1,2,4,5). Surfactant protein D (SP-D) is a crucial PRR that significantly contributes to pulmonary innate immunity by recognizing and binding to glycans present on the surfaces of various pathogens (6–8). Other PRRs, such as SP-A and mannose-binding lectin (MBL), also play essential roles in immune defense by recognizing distinct microbial components and initiating appropriate immune responses (9–11).

Among the various components of the innate immune system, SP-D has emerged as a key player in recognizing and binding to pathogenic glycans, thereby facilitating the clearance of harmful microorganisms (12–14). SP-D, a member of the collectin family, is primarily found in the lungs, where it contributes to pulmonary immunity by aggregating pathogens for removal and modulating inflammatory responses (13,15,16). Given its pivotal role, elucidating the mechanisms of SP-D-glycan interactions can

Submitted November 22, 2024, and accepted for publication April 7, 2025.
*Correspondence: m.minkara@northeastern.edu
Editor: Rommie Amaro.
https://doi.org/10.1016/j.bpj.2025.04.007

Please cite this article in press as: Li and Minkara, Decoding SP-D and glycan binding mechanisms using a novel computational workflow, Biophysical Journal (2025), https://doi.org/10.1016/j.bpj.2025.04.007

provide insights into the development of novel therapeutic strategies, such as enhancing SP-D's affinity for specific pathogens or designing SP-D-based therapeutics.

SP-D interacts with various pathogens, including viruses, bacteria, and fungi (17–19). For example, SP-D has been shown to bind to glycans on the surface of the influenza A virus (IAV), contributing to the clearance of the virus from the lungs (20,21). Additionally, SP-D recognizes and binds to surface glycans of *Pseudomonas aeruginosa* (*P. aeruginosa*), an opportunistic bacterium that frequently colonizes the lungs of immunocompromised individuals, such as those with cystic fibrosis (9,22). *P. aeruginosa*'s pili, which are hair-like appendages adorned with surface glycans like pilin glycan, facilitate attachment to host cells and contribute to its pathogenicity (23–27). Moreover, SP-D's interactions with other pathogens, such as *Aspergillus fumigatus* and *Mycobacterium tuberculosis*, highlight its broad-spectrum antimicrobial activity (28,29).

Current research on SP-D-glycan interactions has yielded valuable insights through both experimental and computational studies (30–33). However, significant gaps remain in our understanding of the detailed binding mechanisms and specificities between SP-D and different pathogenic surface glycans at the atomic level. This is primarily due to the vast diversity of surface glycans found on various pathogens and the limited availability of experimentally solved complex structures (34,35). To elucidate the binding mechanisms between SP-D and pathogenic surface glycans in the absence of crystal complex structures, a comprehensive computational modeling workflow capable of accurately predicting complex structures is essential.

In this study, we propose a novel computational modeling workflow that combines several computational modeling methods, including induced fit docking, molecular mechanics/generalized Born surface area (MMGBSA) binding free energy calculations, and binding pose metadynamics (BPMD) simulations. This workflow is designed to overcome the limitations of traditional docking approaches and provide a more comprehensive understanding of SP-D-glycan interactions. The main objectives of this study are threefold: 1) to develop and validate a comprehensive computational modeling workflow for predicting stable complex structures of SP-D with various pathogenic surface glycans; 2) to identify the key binding sites and mechanisms involved in SP-D's recognition of glycans; and 3) to predict novel pathogenic surface glycan binders using the developed workflow, such as pilin glycan from *P. aeruginosa*. By achieving these objectives, we aim to significantly enhance our understanding of the role played by SP-D in the innate immune system, facilitating the rational design of engineered SP-D variants with improved binding affinity and specificity for therapeutic applications. Moreover, the computational modeling workflow developed in this study has the potential for broader applicability in investigating protein-glycan interactions in various other biological contexts, extending the impact of this research beyond the specific realm of SP-D.

MATERIALS AND METHODS

Viral glycan fragment library construction

The computational workflow started by the construction of a viral glycan fragment library using the GLYCAM-Web server (https://glycam.org/). This library consisted of 34 glycans commonly observed in protein-glycan experimentally solved crystal structures, with detailed information on each glycan fragment provided in Table S1. The initial three-dimensional (3D) structures of these glycans were generated in PDB format and subsequently converted to SDF format using Maestro within the Schrodinger Suite to facilitate induced fit docking (36).

Induced fit docking

To explore the binding mechanisms between SP-D and the glycans, we employed the induced fit docking protocol within the Schrodinger Suite (37). This method was chosen for its ability to account for the flexibility of both the receptor and the ligand, which is essential for accurately modeling the dynamic nature of protein-glycan interactions. In induced fit docking, the wild-type SP-D structure (PDB: 3G83) was used as the receptor, and the Protein Preparation Wizard in the Schrodinger Suite was used to optimize its structure (20,36). The viral glycan fragment library was prepared for induced fit docking using the LigPrep module in the Schrodinger Suite, where all possible ionization states were generated with Epik at pH 7.4 (36). Physiological pH 7.4 was selected to accurately represent the conditions in human tissues, specifically the lung environment, where SP-D interacts with pathogenic glycans. The optimized potentials for liquid simulation (OPLS_2005) force field was employed for both receptor and ligand preparation. A docking grid of $46 \times 46 \times 46$ Å was centered on the primary calcium ion in the carbohydrate recognition domain (CRD) of SP-D. The primary calcium ion was also constrained to ensure proper recognition of the glycans. The extended sampling protocol in induced fit docking was utilized to enhance binding pose sampling.

After induced fit docking, over 1000 binding poses were generated, representing various conformations of SP-D in complex with different glycans. Instead of using default scoring functions to rank the binding poses, we employed MMGBSA binding free energy calculations as a score function to rank all the binding poses. All MMGBSA calculations were conducted via the prime MMGBSA module in the Schrodinger Suite using the OPLS_2005 force field (36). The poses were ranked based on MMGBSA binding free energies, and the top five poses for each glycan were selected for further binding stability evaluation.

Binding pose metadynamics simulations

To assess the stability of the selected binding poses, we performed BPMD simulations. The protein-glycan complexes from the top five binding poses were used as input for BPMD simulations. Each system was parameterized using the S-OPLS force field and solvated with the extended simple point charge (SPC/E) water model within a rectangular box, maintaining a 10 Å distance between the complex and the box boundaries. The systems were neutralized with NaCl. The metadynamics simulations were conducted using the protocol in the BPMD module in the Schrodinger Suite (36,38). During metadynamics, the collective variable was defined as the root mean-square deviation (RMSD) of the glycan's heavy atoms relative to their positions in the induced fit docking output pose. The default biasing parameters recommended by Schrodinger were used, with a hill height of 0.05 kcal/mol and a hill width of 0.02 kcal/mol, approximating one-tenth of the system's thermal energy (kBT). Each metadynamics simulation

Please cite this article in press as: Li and Minkara, Decoding SP-D and glycan binding mechanisms using a novel computational workflow, Biophysical Journal (2025), https://doi.org/10.1016/j.bpj.2025.04.007

was run for 10 ns, with 10 independent simulations performed for each binding pose to improve statistical reliability. This resulted in a total of 17 μs of metadynamics simulations across all glycans. The RMSD of the glycan over the simulations was measured to assess binding stability. Binding poses exhibiting low RMSD fluctuations were considered more stable. For each glycan, the binding pose with the lowest average RMSD was selected as the most stable and used for subsequent analyses of SP-D-glycan interactions.

Alchemical absolute binding free energy calculations

To validate our computational workflow, we performed alchemical absolute binding free energy (ABFE) calculations on five protein-glycan complexes identified from the BPMD stage and compared the results to experimental binding affinity data. The methodology followed the protocol outlined in our previous work, briefly summarized here (39).

We performed ABFE calculations using free energy perturbation to evaluate the binding affinities between SP-D and glycans. A modified version of BAT.py v.2.2, following the protocol of Heinzelmann and Gilson, was applied to the protein-glycan systems (40). Harmonic translational and rotational restraints were imposed to stabilize the glycan within the binding pocket during perturbation, whereas conformational restraints were applied to both the receptor and ligand. The simulations were conducted across 12 λ windows, using Gaussian quadrature to decouple ligand Lennard-Jones and charge interactions. Additional restraint contributions were computed across 16 windows, with the total ABFE calculated as the sum of the free energy components. Data collection occurred over 10 ns per window, leading to a total simulation time of 1280 ns per system. The results were processed using the multistate Bennett acceptance ratio and corrected to the standard state.

Molecular dynamics simulations

To further investigate the interactions between three collectins—SP-D, MBL, and SP-A—and the pilin glycan from *P. aeruginosa*, we conducted extensive unbiased molecular dynamics (MD) simulations. The corresponding pilin glycan's 2D structure and 3D structure are shown in Figs. S1 and S2. Since there is no standard force field available for the pilin glycan, we first assigned partial charges using the restrained electrostatic potential approach (41). This was done using the B3LYP/6-311++G** basis set with an optimized structure in Gaussian 16 (42). Additional force field parameters were generated by Antechamber based on the generalized Amber force field (GAFF2) topology (43,44). The SP-D and MBL structures were retrieved from the PDB (PDB: 3G83 and 1UHP, respectively), whereas the human SP-A structure was generated via homology modeling using SWISSMODEL, with the rat SP-A structure (PDB: 5FFT) serving as the template (20,45–47). Each collectin's complex structure was obtained using our computational workflow, which was then used as the starting structure for the MD simulations.

System preparation was performed using the tleap module from AmberTools23, where hydrogen atoms were added to the structures (43). The Amber ff19SB force field was used to parameterize the proteins, whereas the previously generated parameters were applied to the pilin glycan (48). Each protein-glycan complex was solvated in an optimal point charge (OPC) water box, with a minimum distance of 10 Å between the complex and the box edges (49). Na^+ and Cl^- ions were added to neutralize the system, and the ionic strength was adjusted to 0.15 M NaCl to mimic physiological conditions.

The MD simulations followed the same protocol described in our previous work (39). Initially, a two-stage energy minimization was performed: first, restraining the protein-glycan complex with a force constant of 50 kcal/(mol·Å^2), followed by unrestrained minimization. This was followed by a two-phase equilibration process. In the first phase, the system was heated from 0 to 298 K over 2 ns in the NVT ensemble, applying harmonic restraints of 50 kcal/(mol·Å^2). The second phase involved equilibration at 298 K and 1 bar in the NPT ensemble for 50 ns. Temperature control was achieved using Langevin dynamics, and pressure was maintained with a Monte Carlo barostat (50–52). SHAKE was employed to constrain hydrogen bonds, and long-range, nonbonded interactions were computed using the particle mesh Ewald method with a 10 Å cutoff (53). Production MD simulations were conducted for 1000 ns in the NPT ensemble using GPU-accelerated Amber22 (54).

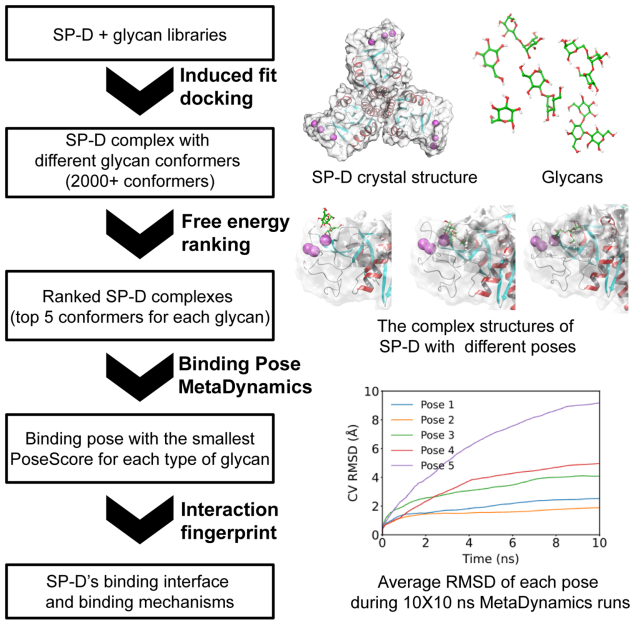

FIGURE 1 Schematic representation of the computational modeling workflow integrating induced fit docking, MMGBSA binding free energy calculations, and BPMD simulations.

RESULTS AND DISCUSSION

Computational modeling workflow for investigating protein-glycan interactions

To investigate the binding mechanisms between SP-D and various glycans, we developed a comprehensive computational modeling workflow that integrates induced fit docking, MMGBSA binding free energy calculations, and BPMD simulations (Fig. 1).

The workflow begins with the construction of a digital library of glycan conformers, which are then subjected to induced fit docking to generate a diverse ensemble of SP-D-glycan complex structures. Although induced fit docking accounts for the flexibility of both the receptor and the ligand, its scoring functions may not always accurately reflect the stability of the binding poses, potentially overlooking energetically favorable conformations. To address this limitation, we employed MMGBSA binding free energy calculations, which, despite being computationally intensive, provide higher accuracy than the traditionally used score functions in estimating binding affinities. This method was used to rank the generated complexes and select the top

Please cite this article in press as: Li and Minkara, Decoding SP-D and glycan binding mechanisms using a novel computational workflow, Biophysical Journal (2025), https://doi.org/10.1016/j.bpj.2025.04.007

five conformers of each glycan type for further analysis. These selected complexes were then evaluated using BPMD simulations, an enhanced sampling technique that efficiently assesses ligand binding stability in solution. BPMD measures the RMSD of the ligand's heavy atoms relative to their initial positions under the influence of a consistent biasing force. Ligands that are not stably bound exhibit higher RMSD fluctuations, as exemplified by pose 5 in Fig. 1. The binding pose with the lowest RMSD, indicative of the highest stability, was subsequently used for detailed analyses of the binding mechanisms.

The workflow integrates three complementary computational methods, each offering distinct advantages, to balance the broad exploration of binding conformations with rigorous assessment of stability. Induced fit docking captures the flexibility of both the receptor and ligand, enabling the generation of diverse conformational ensembles of protein-glycan complexes. We observed that different glycans can induce distinct conformational changes in SP-D, with RMSD values (relative to the unbound protein) ranging from 0.3 to 0.85 Å, as shown in Fig. S3. Larger or more complex glycans generally cause more pronounced rearrangements, underscoring the importance of incorporating protein flexibility when modeling protein-glycan interactions. MMGBSA provides a more accurate and quantitative ranking of binding affinities by incorporating solvation effects and free energy calculations, addressing limitations in traditional docking scoring functions. BPMD further enhances the evaluation by simulating the dynamic behavior of complexes in an explicit solution, delivering a more reliable stability assessment than reliance on MMGBSA free energy values alone. Indeed, we observed cases where the most stable binding pose determined by BPMD diverged from the ranking based on MMGBSA binding free energies, as shown in Table S2. Taking all this together, this workflow is hypothesized to create a robust framework for accurately predicting stable protein-glycan complex structures.

Validation of the computational modeling workflow

To validate the accuracy of our computational workflow, we compared the predicted binding affinities and preferences of various glycans for SP-D with experimental data (32). Table 1 presents detailed descriptions of SP-D's binding preferences for five saccharides, for which experimentally measured IC_{50} values are available. Initially, we employed our workflow to predict the complex structures of different glycans bound to SP-D. Subsequently, we calculated the binding affinities of these complexes using ABFE calculations, as described in our previous study (39).

To assess the agreement between our computational predictions and experimental measurements, we performed a correlation analysis between the computationally predicted binding affinities and the experimentally measured values in Fig. 2, and the corresponding values are listed in Table 1. This analysis yielded a Pearson correlation coefficient of 0.9, indicating a strong positive correlation between the two datasets. The high correlation demonstrates that our computational modeling workflow can accurately predict the binding affinities and preferences of glycans for SP-D, closely aligning with experimental observations. This level of agreement underscores the reliability and robustness of our workflow as a tool for predicting stable protein-glycan complex structures.

TABLE 1 Five glycan fragments and their corresponding experimental IC_{50} values and computationally predicted ΔG for binding with SP-D

Glycan fragment	IC_{50} (mM)	Predicted ΔG (kcal/mol)
DGlcpa1-OH	3.40	−1.96
DManpa1-OH	4.10	−0.33
DGlcpa1-4DGlcpa1-OH	2.50	−2.85
DGalpb1-OH	13.00	0.42
DGlcpNAcb1-OH	9.80	0.90

Identification of primary and secondary binding sites in SP-D

Using our validated computational workflow, we predicted the stable complex structures of various glycans bound to SP-D and investigated their binding mechanisms. We first identified the primary binding sites within the CRD of

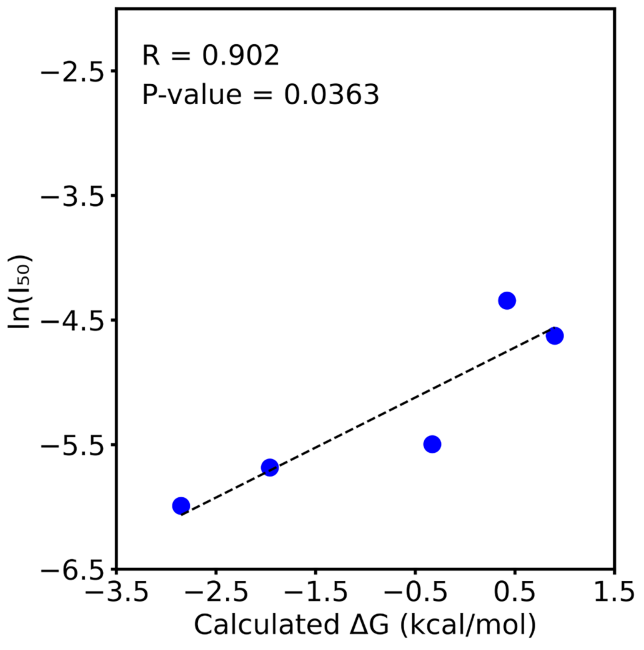

FIGURE 2 Correlation between computationally predicted binding affinities using ABFE calculations and experimentally measured values, yielding a Pearson correlation coefficient of 0.9.

Please cite this article in press as: Li and Minkara, Decoding SP-D and glycan binding mechanisms using a novel computational workflow, Biophysical Journal (2025), https://doi.org/10.1016/j.bpj.2025.04.007

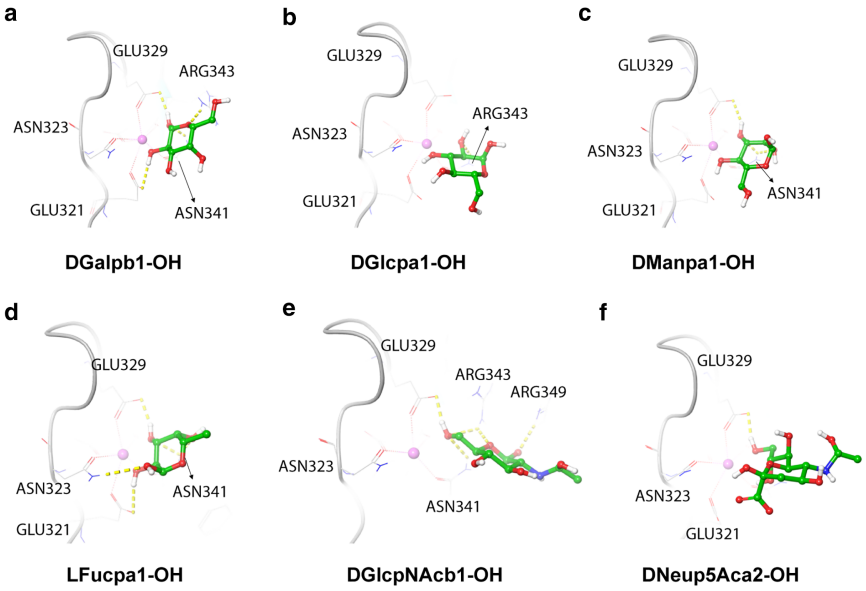

FIGURE 3 Atomic interaction between SP-D and different monosaccharides, including (*a*) DGalpb1-OH, (*b*) DGlcpa1-OH, (*c*) DManpa1-OH, (*d*) LFucpa1-OH, (*e*) DGlcpNAcb1-OH, and (*f*) DNeup5Aca2-OH. The CA401 is shown in a magenta sphere. The yellow dashed lines represent hydrogen bonds.

SP-D, centered around a primary calcium ion and comprising residues Glu321, Glu329, Asn341, and the calcium ion itself (Fig. 3). Monosaccharides interact with these residues through hydrogen bonding and chelation with the calcium ion. The primary binding site is consistently involved in all stable binding poses, underscoring its critical role in the recognition and binding of glycans by SP-D.

As the glycan size increases from monosaccharides to disaccharides and oligosaccharides, additional interactions with a secondary binding site further stabilize the binding. A heatmap analysis of the hydrogen bond occupancy between saccharides and residues in the SP-D CRD reveals that, in addition to the primary binding site residues, several adjacent residues from the secondary binding site, including Asp325, Glu333, Phe335, Thr336, Arg343, Glu347, and Arg349, are involved in saccharide binding (Fig. 4). Notably, our previous study demonstrated the molecular mechanisms by which natural variants Asp325Ala and Arg343Val, located in the secondary binding site, enhance SP-D's binding with the surface glycan from IAV (33). This finding highlights the importance of the secondary binding site in modulating SP-D's binding affinity and specificity toward different glycan targets.

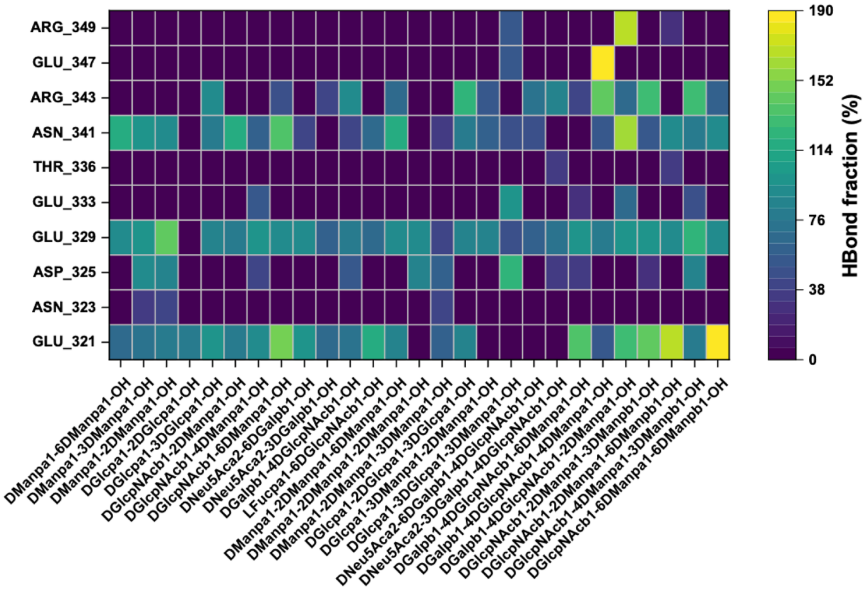

FIGURE 4 Heatmap of the hydrogen bond fraction between SP-D and 12 disaccharides and 15 oligosaccharides.

Please cite this article in press as: Li and Minkara, Decoding SP-D and glycan binding mechanisms using a novel computational workflow, Biophysical Journal (2025), https://doi.org/10.1016/j.bpj.2025.04.007

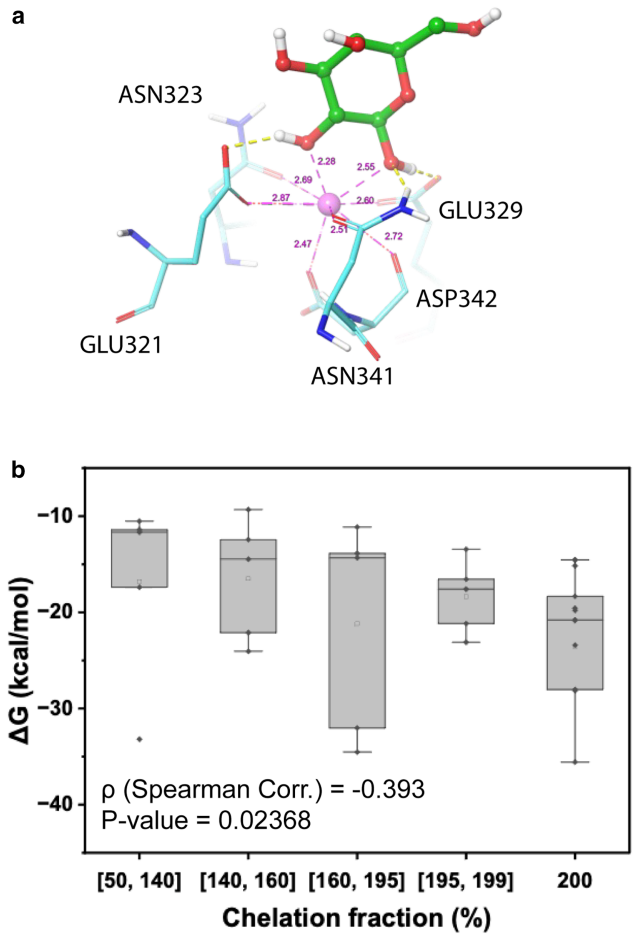

FIGURE 5 (*a*) Coordination geometry of the calcium ion with glycan hydroxyl groups and surrounding SP-D residues. (*b*) Spearman correlation between chelation occupancy and MMGBSA binding free energies, illustrating an inverse relationship.

Role of calcium chelation in SP-D-glycan binding

A detailed examination of the most stable binding conformations of all glycans revealed a ubiquitous calcium chelation mode that plays a pivotal role in the binding affinity between SP-D and glycans (Fig. 5). This chelation mode involves the coordination of two hydroxyl groups from the glycan with the calcium ion in conjunction with five coordinating residues surrounding the primary calcium ion (Fig. 5 *a*). The geometry of this chelation complex is highly conserved among the stable binding poses, suggesting its importance in maintaining the structural integrity and specificity of SP-D-glycan interactions.

To quantitatively assess the relationship between the stability of the calcium chelation and the binding affinity, we performed a correlation analysis between the chelation occupancy and the MMGBSA binding free energies derived from the BPMD trajectories. The chelation occupancy represents the fraction of simulation time during which the glycan hydroxyl groups remain coordinated with the primary calcium ion. Our analysis yielded a Spearman correlation coefficient of -0.393 ($p = 0.002$) (Fig. 5 *b*), indicating a significant inverse relationship between chelation stability and binding free energy. A chelation occupancy of 200% corresponds to both hydroxyl groups from the glycan being stably chelated with the primary calcium ion throughout the entire BPMD simulation. This high chelation occupancy is associated with more negative binding free energies, signifying stronger and more thermodynamically favorable binding.

These findings underscore the critical role of the calcium chelation mode in driving high-affinity interactions between SP-D and glycans. The stable coordination of saccharide hydroxyl groups with the primary calcium ion contributes to the proper orientation and stabilization of the glycan within the binding site, facilitating optimal interactions with the surrounding residues.

Identifying potent immunoprotein binders for pathogenic surface glycans

To demonstrate the applicability of our computational modeling workflow in predicting novel pathogenic surface glycan binders, we applied it to study the interactions between the pilin glycan of *P. aeruginosa* and three major human immunoproteins: SP-A, SP-D, and MBL. *P. aeruginosa* is a prevalent pathogen in immunocompromised patients, particularly those with cystic fibrosis affecting the lungs. Its pili, hair-like structures adorned with surface glycans, facilitate attachment to host cells. Identifying the immunoprotein most capable of effectively binding to the pilin glycan can provide crucial insights into the innate immune response against *P. aeruginosa* infection and guide the development of targeted therapies.

We predicted the stable binding of the pilin glycan to each immunoprotein using our computational workflow, followed by extensive MD simulations to assess the dynamic behavior and binding stability of these complexes. We analyzed the shortest distances between the pilin glycan and the primary calcium ion in the three immunoproteins to evaluate their binding stabilities. The distance curves, illustrated in Figs. 6, 7, and 8, revealed that SP-D exhibits the most stable binding with the pilin glycan, maintaining a consistent interaction throughout the 1000 ns MD simulation (Fig. 6). In contrast, the pilin glycan dissociates from SP-A and MBL after approximately 600 and 350 ns of MD simulation (Figs. 7 and 8), respectively. These results suggest that SP-D is potentially the most potent immunoprotein for binding the pilin glycan from *P. aeruginosa*. Future studies combining computational predictions with experimental investigations will enhance our understanding of protein-glycan interactions and facilitate the development of targeted therapies against pathogens like *P. aeruginosa*.

Our computational modeling workflow has proven to be a powerful tool for accurately predicting stable protein-glycan

Please cite this article in press as: Li and Minkara, Decoding SP-D and glycan binding mechanisms using a novel computational workflow, Biophysical Journal (2025), https://doi.org/10.1016/j.bpj.2025.04.007

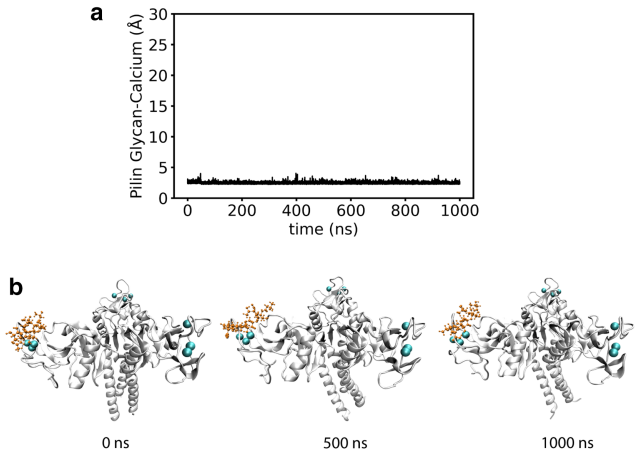

FIGURE 6 (*a*) Shortest distances between pilin glycan and primary calcium ion of SP-D. (*b*) Representative conformations from 0, 500, and 1000 ns show how pilin glycan interacts with the SP-D.

complex structures and identifying key residues involved in the binding process. The identification of primary and secondary binding sites in SP-D, along with the discovery of the correlation between calcium chelation stability and binding affinity, provides valuable insights into the binding mechanisms between SP-D and pathogenic surface glycans. Additionally, the application of our workflow to predict the binding of the pilin glycan from *P. aeruginosa* to human immunoproteins highlights its potential in identifying novel therapeutic targets.2

CONCLUSIONS

In this study, we developed a comprehensive computational modeling workflow that integrates induced fit docking, MMGBSA binding free energy calculations, and BPMD simulations to predict stable protein-glycan complex structures. This workflow was validated against experimental data, demonstrating its reliability in predicting glycan binding preferences and establishing it as a valuable tool for studying protein-glycan interactions.

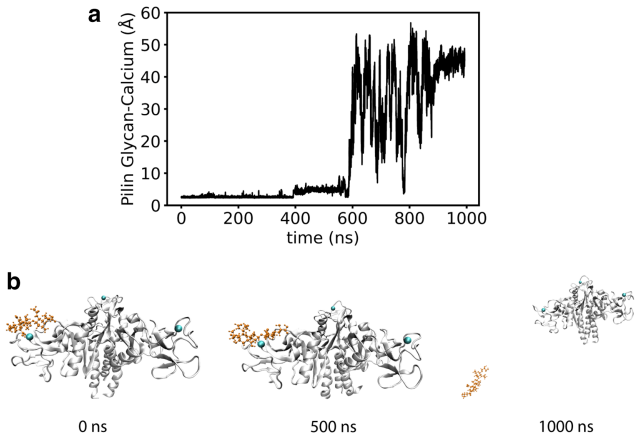

FIGURE 7 (*a*) Shortest distances between pilin glycan and primary calcium ion of SP-A. (*b*) Representative conformations from 0, 500, and 1000 ns show how pilin glycan interacts with the SP-A.

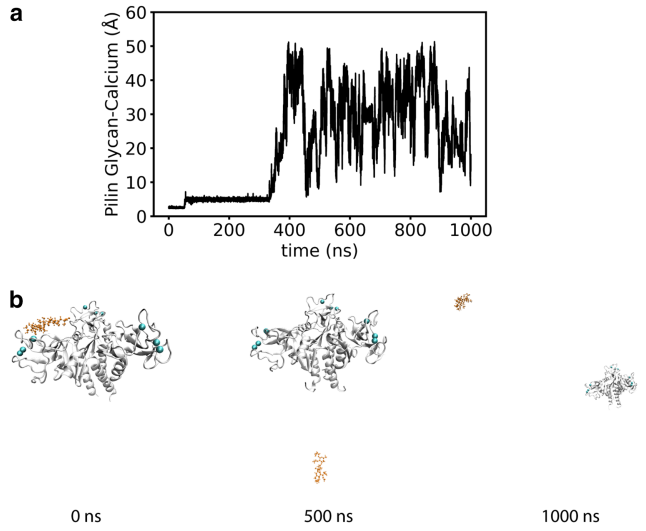

FIGURE 8 (*a*) Shortest distances between pilin glycan and primary calcium ion of MBL. (*b*) Representative conformations from 0, 500, and 1000 ns show how pilin glycan interacts with the MBL.

Through this workflow, we identified the primary and secondary binding sites in SP-D, which are crucial for glycan recognition and binding. Notably, our previous study found that the D325A and R343V variants in SP-D, located in the secondary binding site, enhance SP-D's binding with an oligosaccharide from IAV. This highlights the secondary binding site's importance in modulating SP-D's binding affinity and specificity toward different glycan targets. Additionally, we discovered a ubiquitous calcium chelation mode correlating with high binding affinity, providing a key mechanism for stable and specific interactions between SP-D and its glycan targets.

The successful application of our workflow to predict the binding of pilin glycan from *P. aeruginosa* to different immunoproteins underscores its potential for identifying novel pathogenic surface glycan binders. Our findings indicate that SP-D exhibits the most stable binding with pilin glycan among SP-A, SP-D, and MBL, suggesting that SP-D may play a critical role in the innate immune response against *P. aeruginosa* infection in the lung. This knowledge can inform future experimental studies aimed at designing engineered SP-D variants with enhanced binding affinity and specificity for *P. aeruginosa* and other pathogens, guiding the development of SP-D-based therapies.

In conclusion, our study presents a robust computational modeling workflow that elucidates the binding mechanisms between SP-D and glycans. These findings enhance our understanding of SP-D's role in the innate immune response and lay the groundwork for future applications in therapeutic development targeting protein-glycan interactions.

Please cite this article in press as: Li and Minkara, Decoding SP-D and glycan binding mechanisms using a novel computational workflow, Biophysical Journal (2025), https://doi.org/10.1016/j.bpj.2025.04.007

ACKNOWLEDGMENTS

The authors appreciate the financial support from Northeastern University start-up funds, National Science Foundation (NSF) CAREER Award #2338401, and National Institutes of Health (NIH) MIRA #1R35GM155340. We are grateful to the Discovery Cluster of Northeastern University for computer time and facilities. This work also used Delta GPU at the National Center for Supercomputing Applications (NCSA) through allocation CHE220072 from the Advanced Cyberinfrastructure Coordination Ecosystem: Services & Support (ACCESS) program, which is supported by National Science Foundation grants #2138259, #2138286, #2138307, #2137603, and #2138296 (55). We acknowledge Dr. Elizabeth Andrews (E.A.) for making the materials accessible to M.S.M.

AUTHOR CONTRIBUTIONS

M.S.M. provided funding to support this work, supervised the work, and revised the manuscript. D.L. designed the research and carried out all simulations. D.L. collected and analyzed the data and wrote the manuscript.

DECLARATION OF INTERESTS

The authors declare no competing interests.

DECLARATION OF GENERATIVE AI AND AI-ASSISTED TECHNOLOGIES IN THE WRITING PROCESS

During the preparation of this work, the authors used Microsoft Word editing tools, Grammarly, and ChatGPT to assist in identifying grammar issues and improving clarity. After using these tools, the authors reviewed and edited the content as needed and take full responsibility for the content of the publication.

SUPPORTING MATERIAL

Supporting material can be found online at https://doi.org/10.1016/j.bpj.2025.04.007.

REFERENCES

1. Takeuchi, O., and S. Akira. 2010. Pattern recognition receptors and inflammation. *Cell.* 140:805–820. https://doi.org/10.1016/j.cell.2010.01.022.
2. Li, D., and M. Wu. 2021. Pattern recognition receptors in health and diseases. *Signal Transduct. Targeted Ther.* 6:291. https://doi.org/10.1038/s41392-021-00687-0.
3. Kumagai, Y., and S. Akira. 2010. Identification and functions of pattern-recognition receptors. *J. Allergy Clin. Immunol.* 125:985–992. https://doi.org/10.1016/j.jaci.2010.01.058.
4. Akira, S., and H. Hemmi. 2003. Recognition of pathogen-associated molecular patterns by TLR family. *Immunol. Lett.* 85:85–95. https://doi.org/10.1016/s0165-2478(02)00228-6.
5. Roh, J. S., and D. H. Sohn. 2018. Damage-Associated Molecular Patterns in Inflammatory Diseases. *Immune Netw.* 18:e27. https://doi.org/10.4110/in.2018.18.e27.
6. Hartl, D., and M. Griese. 2006. Surfactant protein D in human lung diseases. *Eur. J. Clin. Invest.* 36:423–435. https://doi.org/10.1111/j.1365-2362.2006.01648.x.
7. Crouch, E., S. F. Kuan, and A. Persson. 1994. Surfactant Protein-D - Possible Roles in Pulmonary Host-Defense. *Prog. Retin. Res.* 27:132–140.
8. Holmskov, U., S. Thiel, and J. C. Jensenius. 2003. Collectins and ficolins: Humoral lectins of the innate immune defense. *Annu. Rev. Immunol.* 21:547–578. https://doi.org/10.1146/annurev.immunol.21.120601.140954.
9. Bufler, P., B. Schmidt, …, M. Griese. 2003. Surfactant protein A and D differently regulate the immune response to nonmucoid Pseudomonas aeruginosa and its lipopolysaccharide. *Am. J. Respir. Cell Mol. Biol.* 28:249–256. https://doi.org/10.1165/rcmb.4896.
10. Nourkami-Tutdibi, N., K. Freitag, …, E. Tutdibi. 2021. Genetic Association With Pseudomonas aeruginosa Acquisition in Cystic Fibrosis: Influence of Surfactant Protein D and Mannose-Binding Lectin. *Front. Immunol.* 12:587313. https://doi.org/10.3389/fimmu.2021.587313.
11. Holmskov, U., R. Malhotra, …, J. C. Jensenius. 1994. Collectins: collagenous C-type lectins of the innate immune defense system. *Immunol. Today.* 15:67–74. https://doi.org/10.1016/0167-5699(94)90136-8.
12. Griese, M. 1999. Pulmonary surfactant in health and human lung diseases: state of the art. *Eur. Respir. J.* 13:1455–1476. https://doi.org/10.1183/09031936.99.13614779.
13. Colmorten, K. B., A. B. Nexoe, and G. L. Sorensen. 2019. The Dual Role of Surfactant Protein-D in Vascular Inflammation and Development of Cardiovascular Disease. *Front. Immunol.* 10:2264. https://doi.org/10.3389/fimmu.2019.02264.
14. Kishore, U., T. J. Greenhough, …, T. Chakraborty. 2006. Surfactant proteins SP-A and SP-D: Structure, function and receptors. *Mol. Immunol.* 43:1293–1315. https://doi.org/10.1016/j.molimm.2005.08.004.
15. McCormack, F. X., and J. A. Whitsett. 2002. The pulmonary collectins, SP-A and SP-D, orchestrate innate immunity in the lung. *J. Clin. Investig.* 109:707–712. https://doi.org/10.1172/Jci200215293.
16. Hartshorn, K. L., M. R. White, …, E. C. Crouch. 2010. Viral aggregating and opsonizing activity in collectin trimers. *Am. J. Physiol.* 298:L79–L88. https://doi.org/10.1152/ajplung.00223.2009.
17. Madan, T., P. Eggleton, …, K. B. Reid. 1997. Binding of pulmonary surfactant proteins A and D to Aspergillus fumigatus conidia enhances phagocytosis and killing by human neutrophils and alveolar macrophages. *Infect. Immun.* 65:3171–3179. https://doi.org/10.1128/iai.65.8.3171-3179.1997.
18. Allen, M. J., R. Harbeck, …, R. J. Mason. 1999. Binding of rat and human surfactant proteins A and D to Aspergillus fumigatus conidia. *Infect. Immun.* 67:4563–4569. https://doi.org/10.1128/IAI.67.9.4563-4569.1999.
19. Hartshorn, K. L., E. Crouch, …, K. N. Sastry. 1998. Pulmonary surfactant proteins A and D enhance neutrophil uptake of bacteria. *Am. J. Physiol.* 274:L958–L969. https://doi.org/10.1152/ajplung.1998.274.6.L958.
20. Crouch, E., K. Hartshorn, …, J. Head. 2009. Recognition of Mannosylated Ligands and Influenza A Virus by Human Surfactant Protein D: Contributions of an Extended Site and Residue 343. *Biochemistry.* 48:3335–3345. https://doi.org/10.1021/bi8022703.
21. Hillaire, M. L. B., H. P. Haagsman, …, M. van Eijk. 2013. Pulmonary Surfactant Protein D in First-Line Innate Defence against Influenza A Virus Infections. *J. Innate Immun.* 5:197–208. https://doi.org/10.1159/000346374.
22. Hou, X., X. Zhang, and Z. Zhang. 2022. Role of surfactant protein-D in ocular bacterial infection. *Int. Ophthalmol.* 42:3611–3623. https://doi.org/10.1007/s10792-022-02354-x.
23. Castric, P., F. J. Cassels, and R. W. Carlson. 2001. Structural characterization of the Pseudomonas aeruginosa 1244 pilin glycan. *J. Biol. Chem.* 276:26479–26485. https://doi.org/10.1074/jbc.M102685200.
24. Liu, H., Y. Zhang, …, X. Li. 2017. Total Synthesis of Pseudomonas aeruginosa 1244 Pilin Glycan via de Novo Synthesis of Pseudaminic Acid. *J. Am. Chem. Soc.* 139:13420–13428. https://doi.org/10.1021/jacs.7b06055.
25. Craig, L., M. E. Pique, and J. A. Tainer. 2004. Type IV pilus structure and bacterial pathogenicity. *Nat. Rev. Microbiol.* 2:363–378. https://doi.org/10.1038/nrmicro885.

26. Smedley, J. G., 3rd, E. Jewell, …, P. Castric. 2005. Influence of pilin glycosylation on Pseudomonas aeruginosa 1244 pilus function. *Infect. Immun.* 73:7922–7931. https://doi.org/10.1128/IAI.73.12.7922-7931.2005.

27. Ramphal, R., J. C. Sadoff, …, J. D. Silipigni. 1984. Role of Pili in the Adherence of Pseudomonas-Aeruginosa to Injured Tracheal Epithelium. *Infect. Immun.* 44:38–40. https://doi.org/10.1128/Iai.44.1.38-40.1984.

28. Wong, S. S. W., M. Rani, …, V. Aimanianda. 2018. Fungal melanin stimulates surfactant protein D-mediated opsonization of and host immune response to spores. *J. Biol. Chem.* 293:4901–4912. https://doi.org/10.1074/jbc.M117.815852.

29. Ferguson, J. S., D. R. Voelker, …, L. S. Schlesinger. 1999. Surfactant Protein D Binds to Mycobacterium tuberculosis Bacilli and Lipoarabinomannan via Carbohydrate-Lectin Interactions Resulting in Reduced Phagocytosis of the Bacteria by Macrophages. *J. Immunol.* 163:312–321.

30. Zhang, J. L., Q. C. Zheng, and H. X. Zhang. 2010. Unbinding of glucose from human pulmonary surfactant protein D studied by steered molecular dynamics simulations. *Chem. Phys. Lett.* 484:338–343. https://doi.org/10.1016/j.cplett.2009.12.022.

31. Zhang, J., Q. Zheng, and H. Zhang. 2010. Insight into the Dynamic Interaction of Different Carbohydrates with Human Surfactant Protein D: Molecular Dynamics Simulations. *J. Phys. Chem. B.* 114:7383–7390. https://doi.org/10.1021/jp9113078.

32. Crouch, E., Y. Tu, …, K. Hartshorn. 2005. Ligand specificity of human surfactant protein D - Expression of a mutant trimeric collectin that shows enhanced interactions with influenza a virus. *J. Biol. Chem.* 280:17046–17056. https://doi.org/10.1074/jbc.M413932200.

33. Li, D., and M. S. Minkara. 2022. Elucidating the enhanced binding affinity of a double mutant SP-D with trimannose on the influenza A virus using molecular dynamics. *Comput. Struct. Biotechnol. J.* 20:4984–5000. https://doi.org/10.1016/j.csbj.2022.08.045.

34. Watanabe, Y., J. D. Allen, …, M. Crispin. 2020. Site-specific glycan analysis of the SARS-CoV-2 spike. *Science.* 369:330–333. https://doi.org/10.1126/science.abb9983.

35. Yuan, Y., D. Cao, …, G. F. Gao. 2017. Cryo-EM structures of MERS-CoV and SARS-CoV spike glycoproteins reveal the dynamic receptor binding domains. *Nat. Commun.* 8:15092. https://doi.org/10.1038/ncomms15092.

36. Schrödinger, L., (2023). Schrödinger Release 2023-2: Maestro.

37. Miller, E. B., R. B. Murphy, …, R. A. Friesner. 2021. Reliable and Accurate Solution to the Induced Fit Docking Problem for Protein-Ligand Binding. *J. Chem. Theor. Comput.* 17:2630–2639. https://doi.org/10.1021/acs.jctc.1c00136.

38. Fusani, L., D. S. Palmer, …, I. D. Wall. 2020. Exploring Ligand Stability in Protein Crystal Structures Using Binding Pose Metadynamics. *J. Chem. Inf. Model.* 60:1528–1539. https://doi.org/10.1021/acs.jcim.9b00843.

39. Li, D., and M. S. Minkara. 2024. Comparative Assessment of Water Models in Protein-Glycan Interaction: Insights from Alchemical Free Energy Calculations and Molecular Dynamics Simulations. *J. Chem. Inf. Model.* 64:9459–9473. https://doi.org/10.1021/acs.jcim.4c01361.

40. Heinzelmann, G., and M. K. Gilson. 2021. Automation of absolute protein-ligand binding free energy calculations for docking refinement and compound evaluation. *Sci. Rep.* 11:1116. https://doi.org/10.1038/s41598-020-80769-1.

41. Bayly, C. I., P. Cieplak, …, P. A. Kollman. 1993. A Well-Behaved Electrostatic Potential Based Method Using Charge Restraints for Deriving Atomic Charges - the Resp Model. *J. Phys. Chem.* 97:10269–10280. https://doi.org/10.1021/j100142a004.

42. Frisch, M.J., Trucks G.W., … Fox, D. J. Gaussian, Inc., Wallingford CT. 2016. Gaussian 16, Revision C.01.

43. Case, D. A., H. M. Aktulga, …, K. M. Merz, Jr. 2023. The AmberTools. *J. Chem. Inf. Model.* 63:6183–6191. https://doi.org/10.1021/acs.jcim.3c01153.

44. He, X., V. H. Man, …, J. Wang. 2020. A fast and high-quality charge model for the next generation general AMBER force field. *J. Chem. Phys.* 153:114502. https://doi.org/10.1063/5.0019056.

45. Sheriff, S., C. Y. Chang, and R. A. B. Ezekowitz. 1996. Human mannose-binding protein carbohydrate recognition domain trimerizes through a triple alpha-helical coiled-coil. *Nat. Struct. Biol.* 3:103.

46. Goh, B. C., H. Wu, …, F. X. McCormack. 2016. Elucidation of Lipid Binding Sites on Lung Surfactant Protein A Using X-ray Crystallography, Mutagenesis, and Molecular Dynamics Simulations. *Biochemistry.* 55:3692–3701. https://doi.org/10.1021/acs.biochem.6b00048.

47. Waterhouse, A., M. Bertoni, …, T. Schwede. 2018. SWISS-MODEL: homology modelling of protein structures and complexes. *Nucleic Acids Res.* 46:W296–W303. https://doi.org/10.1093/nar/gky427.

48. Tian, C., K. Kasavajhala, …, C. Simmerling. 2020. ff19SB: Amino-Acid-Specific Protein Backbone Parameters Trained against Quantum Mechanics Energy Surfaces in Solution. *J. Chem. Theor. Comput.* 16:528–552. https://doi.org/10.1021/acs.jctc.9b00591.

49. Izadi, S., R. Anandakrishnan, and A. V. Onufriev. 2014. Building Water Models: A Different Approach. *J. Phys. Chem. Lett.* 5:3863–3871. https://doi.org/10.1021/jz501780a.

50. Uberuaga, B. P., M. Anghel, and A. F. Voter. 2004. Synchronization of trajectories in canonical molecular-dynamics simulations: Observation, explanation, and exploitation. *J. Chem. Phys.* 120:6363–6374. https://doi.org/10.1063/1.1667473.

51. Sindhikara, D. J., S. Kim, …, A. E. Roitberg. 2009. Bad Seeds Sprout Perilous Dynamics: Stochastic Thermostat Induced Trajectory Synchronization in Biomolecules. *J. Chem. Theor. Comput.* 5:1624–1631. https://doi.org/10.1021/ct800573m.

52. Åqvist, J., P. Wennerström, …, B. O. Brandsdal. 2004. Molecular dynamics simulations of water and biomolecules with a Monte Carlo constant pressure algorithm. *Chem. Phys. Lett.* 384:288–294. https://doi.org/10.1016/j.cplett.2003.12.039.

53. Ryckaert, J.-P., G. Ciccotti, and H. J. C. Berendsen. 1977. Numerical integration of the cartesian equations of motion of a system with constraints: molecular dynamics of n-alkanes. *J. Comput. Phys.* 23:327–341. https://doi.org/10.1016/0021-9991(77)90098-5.

54. D.A. Case, H. M. A., … P.A. Kollman. 2023. Amber 2023.

55. Boerner, T. J., S. Deems, J. Towns…, 2023. ACCESS: Advancing Innovation: NSF's Advanced Cyberinfrastructure Coordination Ecosystem: Services & Support. *In* Practice and Experience in Advanced Research Computing Association for Computing Machinery https://dl.acm.org/doi/10.1145/3569951.3597559.

Biophysical Journal, Volume *124*

Supplemental information

Decoding SP-D and glycan binding mechanisms using a novel computational workflow

Deng Li and Mona S. Minkara

Supplementary Information: Decoding SP-D and glycan binding mechanisms using a novel computational workflow

Deng Li[1] and Mona S. Minkara[1*]

[1]Department of Bioengineering, Northeastern University, Boston, MA, 02120, USA

[*]Correspondence: Mona S. Minkara, m.minkara@northeastern.edu

Table S1 Viral glycan fragment library.

Glycan fragment	Name
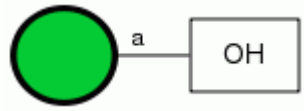	DManpa1-OH
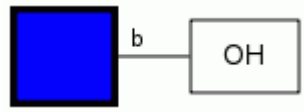	DGlcpNAcb1-OH
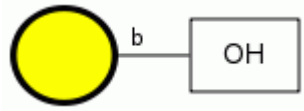	DGalpb1-OH
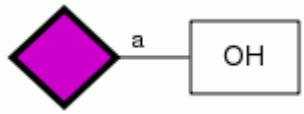	DNeup5Aca2-OH
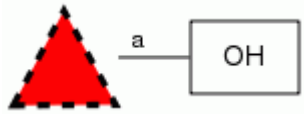	LFucpa1-OH
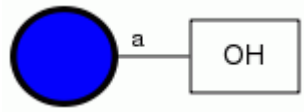	DGlcpa1-OH
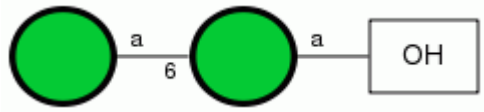	DManpa1-6DManpa1-OH
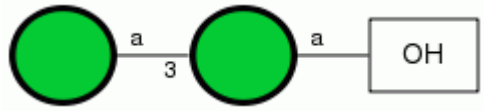	DManpa1-3DManpa1-OH
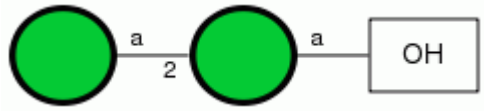	DManpa1-2DManpa1-OH
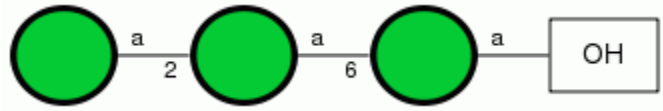	DManpa1-2DManpa1-6DManpa1-OH
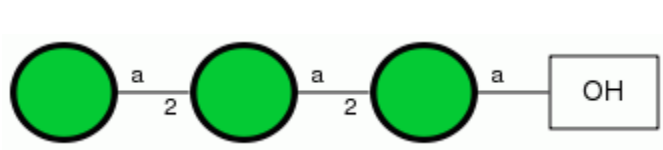	DManpa1-2DManpa1-2DManpa1-OH
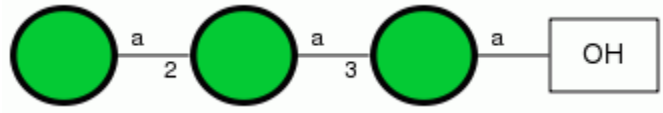	DManpa1-2DManpa1-3DManpa1-OH
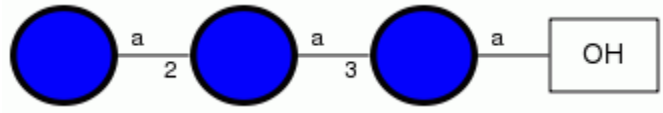	DGlcpa1-2DGlcpa1-3DGlcpa1-OH

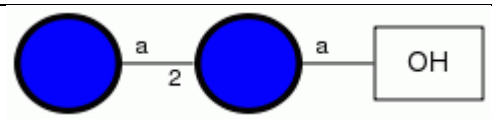	DGlcpa1-2DGlcpa1-OH
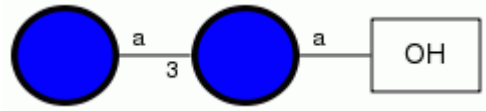	DGlcpa1-3DGlcpa1-OH
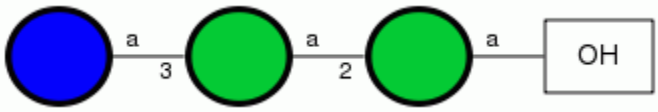	DGlcpa1-3DManpa1-2DManpa1-OH
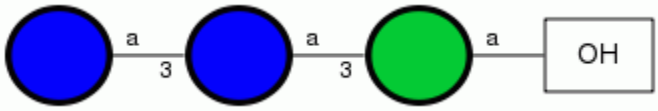	DGlcpa1-3DGlcpa1-3DManpa1-OH
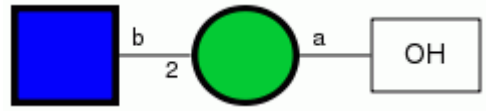	DGlcpNAcb1-2DManpa1-OH
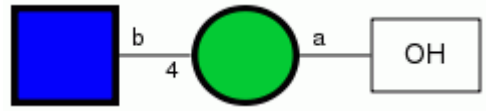	DGlcpNAcb1-4DManpa1-OH
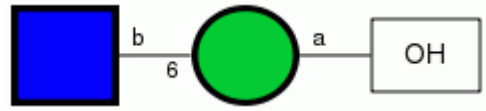	DGlcpNAcb1-6DManpa1-OH
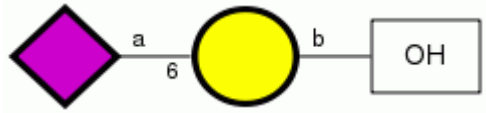	DNeu5Aca2-6DGalpb1-OH
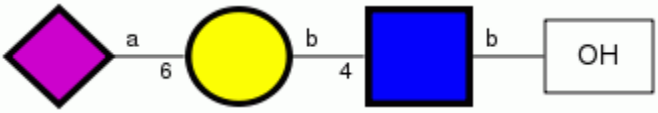	DNeu5Aca2-6DGalpb1- 4DGlcpNAcb1-OH
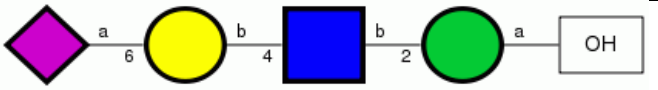	DNeu5Aca2-6DGalpb1- 4DGlcpNAcb1-2DManpa1-OH
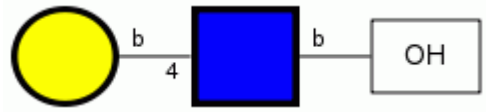	DGalpb1-4DGlcpNAcb1-OH
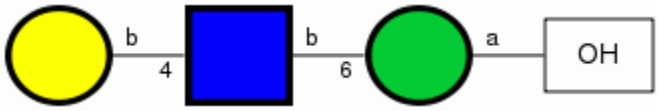	DGalpb1-4DGlcpNAcb1- 6DManpa1-OH
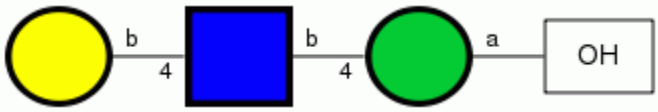	DGalpb1-4DGlcpNAcb1- 4DManpa1-OH
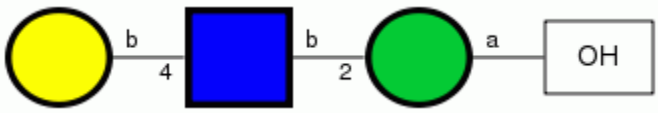	DGalpb1-4DGlcpNAcb1- 2DManpa1-OH

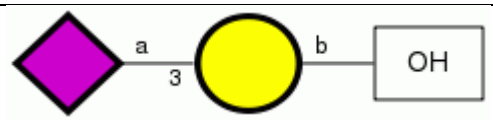	DNeu5Aca2-3DGalpb1-OH
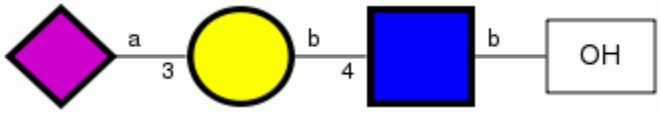	DNeu5Aca2-3DGalpb1-4DGlcpNAcb1-OH
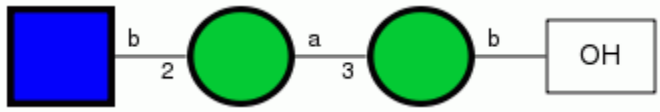	DGlcpNAcb1-2DManpa1-3DManpb1-OH
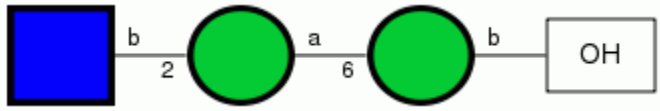	DGlcpNAcb1-2DManpa1-6DManpb1-OH
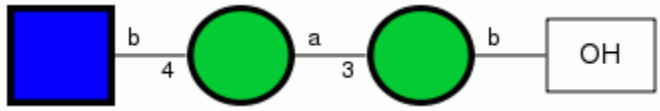	DGlcpNAcb1-4DManpa1-3DManpb1-OH
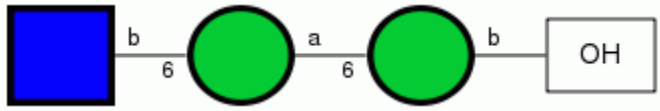	DGlcpNAcb1-6DManpa1-6DManpb1-OH
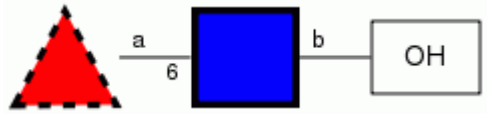	LFucpa1-6DGlcpNAcb1-OH

Table S2. Comparison of MMGBSA dG values and RMSD from binding pose metadynamics (BPMD) simulations for the top 5 poses of glycans.

Glycan	Binding poses	MMGBSA dG (kcal/mol)	RMSD after BPMD (Å)
DGalpb1-4DGlcpNAcb1-6DManpa1-OH	Pose 1	-68.03	2.57
	Pose 2	-75.05	4.92
	Pose 3	-75.20	5.39
	Pose 4	-72.34	5.78
	Pose 5	-63.69	9.13
DGalpb1-OH	Pose 1	-24.64	0.88
	Pose 2	-26.81	1.04
	Pose 3	-25.60	1.33
	Pose 4	-23.81	2.60
	Pose 5	-24.83	6.65
DGlcpNAcb1-2DManpa1-6DManpb1-OH	Pose 1	-74.75	1.54
	Pose 2	-74.41	2.04
	Pose 3	-70.61	2.66
	Pose 4	-77.26	3.11
	Pose 5	-75.09	3.85
DGlcpNAcb1-2DManpa1-OH	Pose 1	-37.30	1.10
	Pose 2	-40.32	1.19
	Pose 3	-53.12	2.56
	Pose 4	-41.34	2.93
	Pose 5	-45.53	3.52
DGlcpNAcb1-4DManpa1-3DManpb1-OH	Pose 1	-51.41	2.28
	Pose 2	-47.34	2.31
	Pose 3	-47.60	4.41
	Pose 4	-47.01	4.99
	Pose 5	-56.63	5.09

Table S2. Continued.

Glycan	Binding poses	MMGBSA dG (kcal/mol)	RMSD after BPMD (Å)
DGlcpNAcb1-4DManpa1-OH	Pose 1	-39.97	1.41
	Pose 2	-39.56	1.42
	Pose 3	-41.54	1.78
	Pose 4	-51.20	2.08
	Pose 5	-38.41	2.44
DGlcpNAcb1-6DManpa1-6DManpb1-OH	Pose 1	-69.83	3.38
	Pose 2	-63.67	3.84
	Pose 3	-71.97	3.93
	Pose 4	-80.79	4.85
	Pose 5	-67.80	5.35
DGlcpNAcb1-6DManpa1-OH	Pose 1	-48.33	1.70
	Pose 2	-48.21	2.06
	Pose 3	-51.77	3.57
	Pose 4	-45.75	3.76
	Pose 5	-50.77	3.81
DGlcpNAcb1-OH	Pose 1	-24.51	0.96
	Pose 2	-26.26	1.11
	Pose 3	-24.37	4.14
	Pose 4	-27.84	4.33
	Pose 5	-25.57	4.65
DGlcpa1-2DGlcpa1-OH	Pose 1	-36.82	1.29
	Pose 2	-39.76	1.97
	Pose 3	-36.86	2.56
	Pose 4	-42.22	2.74
	Pose 5	-38.97	3.17

Table S2. Continued.

Glycan	Binding poses	MMGBSA dG (kcal/mol)	RMSD after BPMD (Å)
DGlcpa1-3DGlcpa1-OH	Pose 1	-36.56	1.80
	Pose 2	-36.71	2.17
	Pose 3	-34.81	2.51
	Pose 4	-31.19	2.71
	Pose 5	-30.60	3.14
DGlcpa1-3DManpa1-2DManpa1-OH	Pose 1	-45.53	2.81
	Pose 2	-51.07	3.24
	Pose 3	-50.92	3.74
	Pose 4	-40.65	3.88
	Pose 5	-43.18	4.93
DGlcpa1-OH	Pose 1	-19.62	0.79
	Pose 2	-21.25	2.47
	Pose 3	-17.02	3.15
	Pose 4	-16.82	3.23
	Pose 5	-23.44	8.27
DManpa1-2DManpa1-2DManpa1-OH	Pose 1	-41.87	1.83
	Pose 2	-36.10	2.47
	Pose 3	-37.46	4.06
	Pose 4	-37.17	4.85
	Pose 5	-42.64	8.98
DManpa1-2DManpa1-3DManpa1-OH	Pose 1	-37.27	2.48
	Pose 2	-40.93	2.51
	Pose 3	-41.90	2.63
	Pose 4	-43.42	3.64
	Pose 5	-53.60	6.92

Table S2. Continued.

Glycan	Binding poses	MMGBSA dG (kcal/mol)	RMSD after BPMD (Å)
DManpa1-2DManpa1-6DManpa1-OH	Pose 1	-48.58	3.10
	Pose 2	-57.37	3.50
	Pose 3	-43.75	3.82
	Pose 4	-47.92	4.38
	Pose 5	-54.01	4.94
DManpa1-2DManpa1-OH	Pose 1	-36.07	2.07
	Pose 2	-35.95	2.44
	Pose 3	-35.66	2.74
	Pose 4	-39.67	3.01
	Pose 5	-34.54	3.53
DManpa1-3DManpa1-OH	Pose 1	-33.73	1.62
	Pose 2	-37.31	1.96
	Pose 3	-35.30	2.27
	Pose 4	-32.69	2.46
	Pose 5	-34.41	2.64
DManpa1-6DManpa1-OH	Pose 1	-37.31	1.01
	Pose 2	-38.46	1.66
	Pose 3	-41.39	1.95
	Pose 4	-38.64	3.20
	Pose 5	-36.72	3.84
DManpa1-OH	Pose 1	-26.31	0.64
	Pose 2	-20.80	0.77
	Pose 3	-26.88	0.83
	Pose 4	-19.73	1.08
	Pose 5	-24.17	1.66

Table S2. Continued.

Glycan	Binding poses	MMGBSA dG (kcal/mol)	RMSD after BPMD (Å)
DNeu5Aca2-3DGalpb1-OH	Pose 1	-45.92	2.16
	Pose 2	-41.90	2.96
	Pose 3	-39.10	3.35
	Pose 4	-44.44	4.44
	Pose 5	-53.26	4.53
DNeu5Aca2-6DGalpb1-OH	Pose 1	-49.17	1.34
	Pose 2	-51.57	2.58
	Pose 3	-54.16	2.82
	Pose 4	-50.48	3.31
	Pose 5	-64.71	3.52
DNeup5Aca2-OH	Pose 1	-28.27	1.81
	Pose 2	-30.61	2.00
	Pose 3	-29.71	2.53
	Pose 4	-30.63	2.94
	Pose 5	-29.76	5.01
LFucpa1-6DGlcpNAcb1-OH	Pose 1	-40.17	1.49
	Pose 2	-41.69	2.07
	Pose 3	-40.39	2.57
	Pose 4	-45.01	2.63
	Pose 5	-47.66	2.67
LFucpa1-OH	Pose 1	-23.27	0.63
	Pose 2	-20.92	0.79
	Pose 3	-21.28	0.82
	Pose 4	-21.24	0.91
	Pose 5	-28.86	0.92

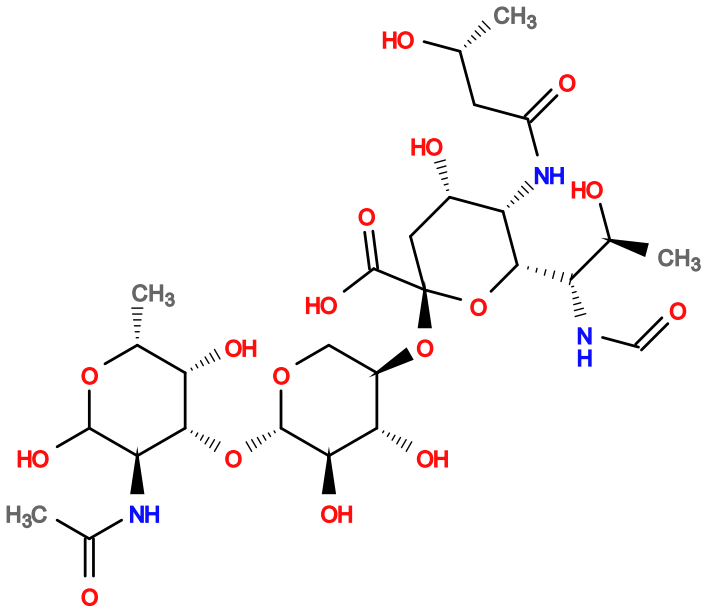

Figure S1. 2D structure of pilin glycan of *Pseudomonas aeruginosa* strain 1244.

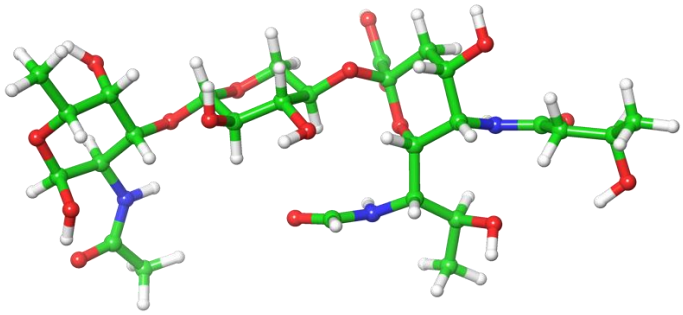

Figure S2. 3D structure of pilin glycan of *Pseudomonas aeruginosa* strain 1244.

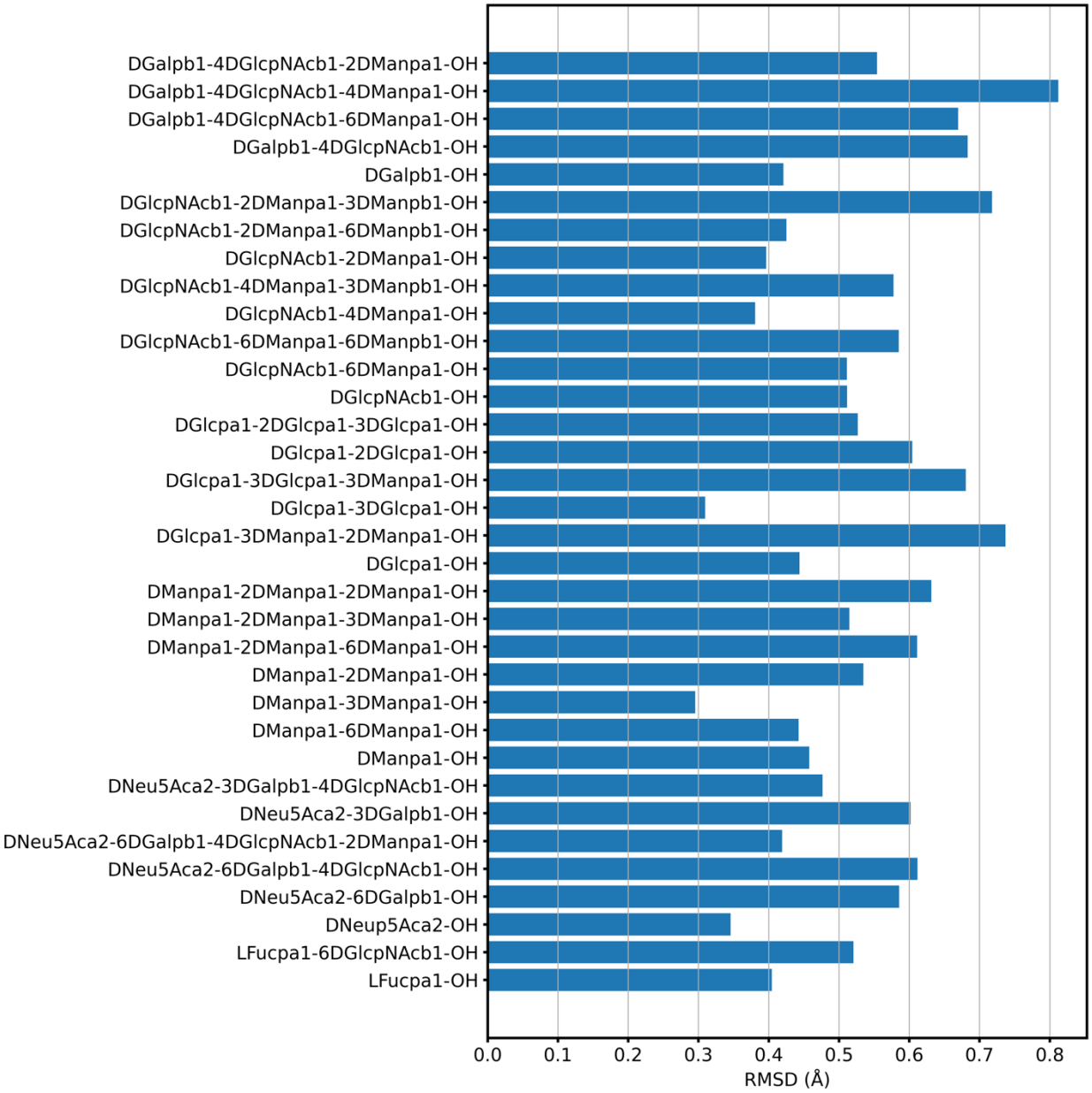

Figure S3. The RMSD of SP-D after induced fit docking (IFD) with different glycans. Higher RMSD values indicate more extensive conformational adjustments within the binding site and thus a more pronounced induced-fit effect.